http://ansinet.com/itj

ITJ

ISSN 1812-5638

INFORMATION TECHNOLOGY JOURNAL

ANSInet
Asian Network for Scientific Information
308 Lasani Town, Sargodha Road, Faisalabad - Pakistan

Information Technology Journal 8 (8): 1160-1169, 2009
ISSN 1812-5638
© 2009 Asian Network for Scientific Information

The Analysis of the Synthetic Range Profile Based on Doppler Filter Bank using FFT

Wei Peng, Xuegang Wang, Kesong Chen and Bin Tang
School of Electronic Engineering, University of Electronic Science and Technology of China,
Chengdu 610054, Sichuan, China

Abstract: A wideband imaging architecture based on subbanding and Doppler filter bank using FFT is developed and its performance is analyzed in detail. The theoretical analysis shows that owing to Doppler dispersion, the target's range profile will produce distortion with the increase in target velocity. The distortion includes range shift and amplitude deformation. At the same time, two related theoretical formulas are deduced for the calculation of the range shift value and evaluation of the amplitude deformation extent of a moving target's range profile formed by the proposed imaging architecture and thereby the maximum critical velocity is derived. When target velocity is less than the maximum critical velocity, a moving target's range profile with acceptable distortion can be obtained. Specific conclusions are verified with some simulations.

Key words: Radar imaging, subbands, wideband Doppler filter bank, target Doppler dispersion, FFT

INTRODUCTION

The High-Range Resolution Profile (HRRP) represents a target's radial backscattering intensity. Compared to a two-dimensional radar image, it is easier to generate owing to the lower cost and less computational complexity. Today, with the increasing sophistication, complexity and diversity of the targets, the demand for the available HRRP has been rising to meet the needs of Automatic Target Classification (ATC) and battle sense (Linde, 2000). However, since various types of narrow band components existing in today's radar systems are unsustainable with wideband signals, it is difficult to transmit or receive a complete instantaneous wideband waveform in a single process (Wehner, 1995; Rabideau, 2002). For example, for an air-to-ground surveillance radar, its most critical task is to separate target returns from ground clutter which generally can be accomplished using Doppler filtering architecture (George, 1998); however, the current Doppler approaches are based on narrowband signal processing. Without a certain form of compensation to prevent the deleterious effects of Doppler dispersion (Zatman, 1998; Pillai *et al*., 2007), which probably causes target migration over a coherent integration time or the deformation of the target range profile, the increase of bandwidth may make conventional Doppler processes no longer possible. However, in many cases, such compensation is very difficult to perform (Perry *et al*., 1999; Torres *et al*., 2000).

An effective alternative is to decompose the wideband signal into subbands (Walbridge and Chadwick, 1999; Morgan and Thi, 1995; Sekiguchi and Kharasawa, 1998), each with a sufficiently small bandwidth that can be processed using the conventional narrowband filter techniques (Peng *et al*., 2008). For example, clutter can be mitigated in each subband using MTI (moving target indication) or STAP (space time adaptive processing) (Malas *et al*., 2002). Then, the outputs of each subband are recombined for the reconstruction of the full wide bandwidth and high resolution signal waveform (Malas *et al*., 2004). Such a target range profile is called Synthetic Range Profile (SRP).

In general, there are two methods of acquiring coherent pulse trains when using subband Doppler technique. One is to separately transmit and receive a certain number of coherent narrow band pulse trains, various in centre frequencies that cover the expected bandwidth. In this case, the key issue is the target motion compensation (Chen *et al*., 2007). The other method is to decompose directly a received coherent wideband pulse train into narrowband components by a set of analysis filters, with the design solution for analysis filters bank as the key technique (Whelan *et al*., 2000). In essence, these two methods can be considered to be equivalent to each other. Some related studies by various researchers have been written for clutter suppression and adaptive processing based on subbanding (Hoffman and Kogon, 2000; Jouny and Culpepper, 1994; Yuan *et al*., 2000).

Narrow radars stress target detection, while wideband radars emphasize the target imaging. Since, a target's SRP is formed by the recombination of the

Corresponding Author: P. Wei, School of Electronic Engineering, University of Electronic Science and Technology of China, 610054, Chengdu, Sichuan, China Tel: 86-28-83200767 Fax: 86-28-83201690

outputs of all subband filter bank, the point of imaging should be taken essential to analyzing the relationships between the Filtered Synthetic Range Profile (FSRP) and subband Doppler filter bank characteristics. Pitifully, so far few researchers have ever discussed related issues. A deeper analysis shows that the mismatch between the target return signals and subband Doppler filter banks, owing to target Doppler dispersion, inevitably causes the performance loss of the FSRP, which includes the power loss and the distortion of the FSRP after recombination. In practical application, mismatches of this type are inevitable simply because these unknown target return signals always vary from subband to subband while all suband Doppler filter architectures, identical with each other, are already fixed in design.

In this study, a wideband imaging radar system, based on the conventional Doppler filter bank architecture (using FFT) and subbanding technique is firstly developed, with a detailed analysis of its performances. The theoretical analysis shows that owing to Doppler dispersion, the target's FSRP will produce power loss and distortion with the increase in target velocity. The power loss fluctuates with the change of the target velocity, which affects the wideband target detection performance. The distortion includes range shift and amplitude deformation of the Filtered Synthetic Range Profile (FSRP), possibly degrading the ATC performance. At the same time, two related theoretical formulas are derived for the calculation of the range shift value and evaluation of the amplitude deformation extent of a moving target's FSRP. After that, the maximum critical velocity of the proposed imaging system is thereby derived, which can determine the scope of application for this imaging architecture. i.e., when target velocity is below the maximum critical velocity, the moving target produces an acceptable distortion of range profile. Finally, we conclude our research by certain simulations to verify our conclusions.

SYNTHETIC WIDEBAND DOPPLER FILTER BANK ARCHITECTURE

Processing procedure: Figure 1 shows the synthetic wideband Doppler filter bank architecture and the complete imaging process for FSRP (In Fig. 2, the role of MTI is to suppress clutter but this study, mainly focused on the effect of Doppler bank on FSRP, thus ignores the role of MTI). As stated previous, considering Doppler filter being inherently a narrowband filter, this presents the motivation for the partitioning of the wideband data into a number of subbands. Each subband can be considered a narrowband signal whose returns individually provide a very coarse range resolution (associated with the subband bandwidth) with the target power residing primarily in a single range bin. As shown in Fig. 1a, each subband target return train within each subband target range bin (for all subbands, the target lies in the same range bin due to the coarse resolution) is treated in parallel by Doppler filter bank. The amplitude and phase values of the filtered target return in a subband can be regarded to consist of two parts. One is the sample of a target's frequency domain response at this subband center frequency. A distortionless SRP (also called original synthetic range profile, ORP) can be obtained by resorting to inverse discrete Fourier transform of the complete set of target frequency response samples across all subbands. The other part, which depends on the interaction between target temporal snapshot vector and the filter bank's architecture, is the main reason causing the distortion of FSRP.

In Fig. 1a, W_n represents weight matrix of dimension M×M associated with the Doppler filter bank of the nth subband, where, $W_n = [w_{n0}, w_{n1}, w_{n2},..., w_{n,M-1}]$ and w_{nk} is a M×1 filter weight vector of the kth filter. In Fig. 1b, the outputs of N subband filter banks form a M×N output array (called Doppler-Subband array). Each complex value

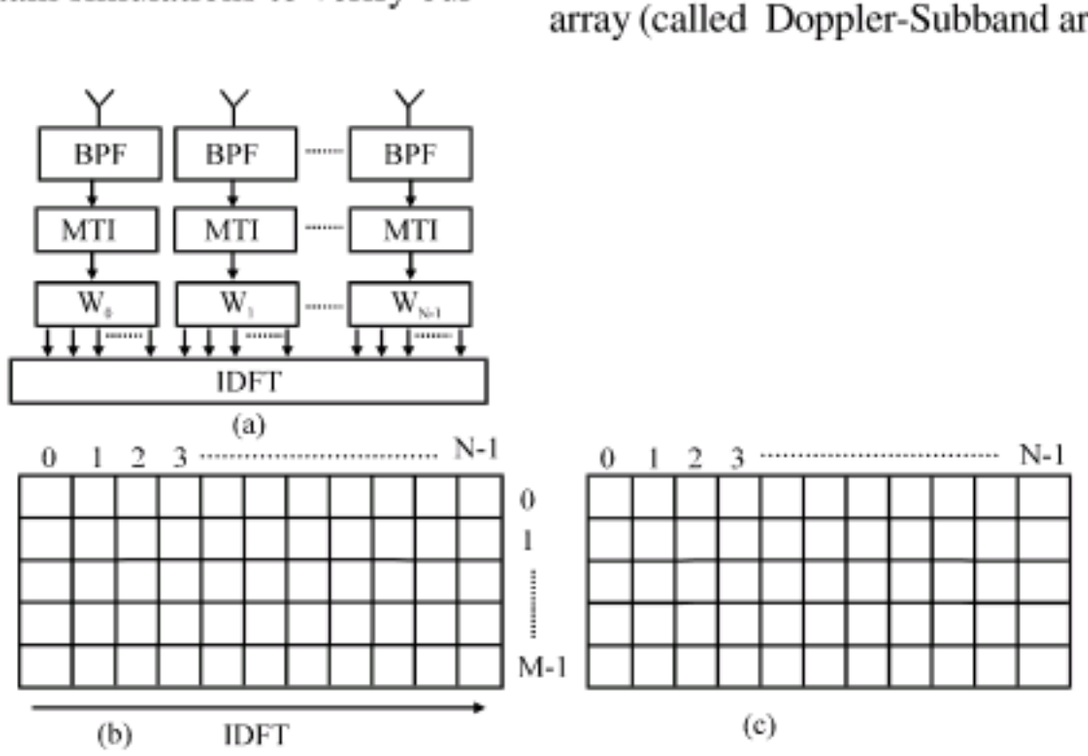

Fig. 1: The general illustration of wideband Doppler filter bank architecture and processing for FSRP, (a) Synthetic wideband Doppler filter bank architecture and (b) Doppler-subband array and (c) Doppler-range array

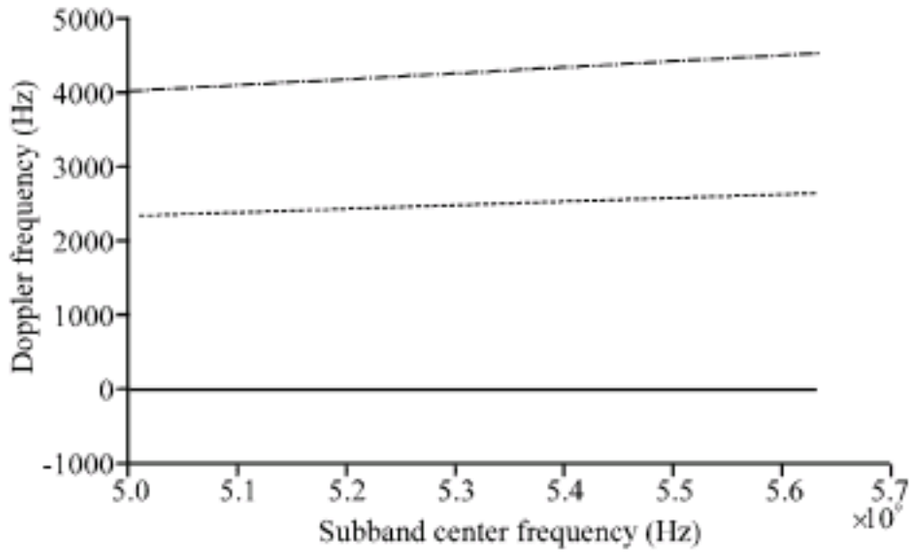

Fig. 2: Change in target Doppler frequency versus change in subband center frequency

within each Doppler-subband cell represents a frequency sample of the target. After the Inverse Discrete Fourier Transform (IDFT) of each row of Doppler-subband array (namely across all subbands), a new array (called Doppler-range array) is formed and each complex value within each cell of this array represents a time sample of the filtered target response, as shown in Fig. 1c. In this way, a synthetic range complex profile (associated with wideband resolution) can be obtained within an individual Doppler bin. Peak detection can be performed, either prior to or after IDFT, within each Doppler bin (associated with wideband resolution). To be specific, peak detection after the IDFT has one single advantage, that is, compared to narrow peak detection in the frequency domain, it can make an additional integration and thus an improved level of peak sharpness within the FSRP.

Target doppler dispersion: According to the Doppler frequency definition in the narrowband radar, i.e., $f_d = 2v_t/\lambda$, where v_t and λ denote target radial velocity and wavelength separately, when the center frequency of each subband changes across subbands, so will the wavelength and, thus, the Doppler frequency. In other words, the target with a constant radial velocity is marked with varying Doppler frequencies from subband to subband, which are also referred to as target Doppler dispersion.

Figure 2 shows variations in target Doppler frequency in pace with those in subband center frequency. In the Fig. 2, the subband number is 64. The first subband center frequency is f_0 = 5GHz and the rest of subband center frequencies are equally spaced and monotonically increasing, i.e., $f_n = f_0 + n\Delta f$ and Δf = 10 MHz. The target velocities are 0 m sec^{-1} (solid line), 70 m sec^{-1} (dashed line) and 120 m sec^{-1} (dash-dot line) separately.

TARGET DOPPLER DISPERSION'S EFFECTS ON FSPR

In the Pulse Doppler (PD) radar system, the most typical component of the Doppler processing is the Doppler filter bank, which can be implemented through a Fast Fourier Transform (FFT) for computational efficiency. In this study, we assume that all Doppler filter banks in every subband are identical and they can be implemented using FFT. In this case, the FFT produces fixed Doppler bin output uniformly spaced in frequency.

Next, we will make a rigorous and complete analysis of target Doppler dispersion effects on FSRP. First, let's assume that there are N subbands with bandwidth ΔB. Let f_n represent the center frequency of the nth subband and assume that the center frequencies are equally spaced and monotonically increasing, i.e., $f_n = f_n + n\Delta f$ and $\Delta f = \Delta B$. Then, f_r represents Pulse Repetition Frequency (PRF) and $T_r = 1/f_r$ represents the Pulse Repetition Interval (PRI). The number of pulses in a CPI (coherent processing interval) is M. In this study, assume that the target has a uniform radial motion with velocity v_t.

The model of the Doppler filter bank outputs in a subband: For simplicity, we assume that the target return signal vector in a subband target range bin only consists of two components. One is the target frequency response sample value at the center frequency of this subband and the other is target temporal snapshot vector. In this way, the target return signal vector can be expressed as:

$$V_{tn} = a_{tn}S_{tn} = a_{tn}[1,\exp\{j2\pi f_{nd}T_r\},\exp\{j2\pi f_{nd}2T_r\},....,\exp\{j2\pi f_{nd}(M-1)T_r\}]^T \quad (1)$$

where, $[\bullet]^T$ denotes the operation of transposition, V_{tn}, a_{tn} and S_{tn} represent the target return signal vector, target frequency response sample value and temporal snapshot vector in the nth subband, respectively. f_{nd} is the target Doppler frequency in the nth subband and

$$f_{nd} = \frac{2v_t}{c}f_n = \frac{2v_t}{c}f_0 + n\frac{2v_t}{c}\Delta f = f_{0d} + n\Delta f_d$$

where, f_{0d} is the Doppler frequency caused by target radial velocity in the first subband.

$$\Delta f_d = \frac{2v_t}{c}\Delta f$$

is caused by target Doppler dispersion and therefore is called Doppler dispersion term in this study.

The weight vector of the kth Doppler filter in the nth subband can be expressed as:

$$w_{nk} = [1 \ \exp\{j2\pi k/M\} \cdots \exp\{j2\pi k(M-1)/M\}]^T \quad (2)$$

Thus, the output of the kth Doppler filter in the nth subband can be obtained:

$$y_{nk} = w_{nk}^H V_{tn} = a_{tn} w_{nk}^H S_{tn} = a_{tn} \sum_{m=0}^{M-1} \exp\{j2\pi(f_{nd}T_r - k/M)m\} = a_{tn}\phi_{nk}(f_{nd}) \quad (3)$$

where, $[\bullet]^H$ denotes the operation of conjugation and transposition and

$$\phi_{nk}(f_{nd}) = w_{nk}^H S_{tn} = \exp\{j\pi(f_{nd}T_r - k/M)(M-1)\}\frac{\sin[\pi(f_{nd}T_r - k/M)M]}{\sin[\pi(f_{nd}T_r - k/M)]} \quad (4)$$

Substituting $f_{nd} = f_{0d} + n\Delta f_d$ into Eq. 4, then we can get:

$$\phi_{nk}(f_{nd}) = \exp\{j\pi[f_{0d} + n\Delta f_d - kf_r/M](M-1)T_r\}\frac{\sin\{\pi[f_{0d} + n\Delta f_d - kf_r/M]MT_r\}}{\sin\{\pi[f_{0d} + n\Delta f_d - kf_r/M]T_r\}} = \theta_{nk}(f_{nd})A_{nk}(f_{nd}) \quad (5)$$

note that here $A_{nk}(f_{nd})$, $\theta_{nk}(f_{nd})$ are the amplitude and phase term of $\phi_{nk}(f_{nd})$, respectively.

The analysis of Doppler filter bank outputs: The expression in Eq. 3 indicates that the output of the kth Doppler filter in the nth subband consists of two terms. One is a_{tn}, or the target frequency response sample value at frequency f_n, which depends exclusively on the target scattering characteristic. The other is $\phi_{nk}(f_{nd})$ that depends on the interaction between target temporal snapshot vector and filter weight vector.

Here, we define T_t as target frequency response sample vector and $T_t = [a_{t0}, a_{t1}, a_{t2},...,a_{t,N-1}]^T$, which represents the target's discrete scattering characteristic in frequency domain within the expected bandwidth. So, the target Original Range Profile (ORP), or the target's distortionless range profile, can be exactly reconstructed by IDFT of target frequency response sample vector, i.e., $h = D^{-1}T_t$, where, h is target's ORP and D^{-1} is the IDFT processing matrix.

$$D = \begin{bmatrix} 1 & 1 & \cdots & 1 \\ 1 & e^{\frac{-j2\pi}{N}} & \cdots & e^{\frac{-j2\pi(N-1)}{N}} \\ \vdots & & & \\ 1 & e^{\frac{-j2\pi(N-1)}{N}} & \cdots & e^{\frac{-j2\pi(N-1)^2}{N}} \end{bmatrix}$$

Target's Filtered Synthetic Range Profile (FSRP): Target's filtered synthetic range profile (FSRP) can be obtained by IDFT of the outputs of all identical Doppler filters across all N subbands, i.e., $h_k = D^{-1}T_{kt}$, where, D^{-1} is the IDFT processing matrix and h_k is the FSRP of the kth Doppler filter and h_k is the output vector formed by collecting the outputs of the kth Doppler filter across N subbands.

According to Eq. 3, we can see,

$$T_{kt} = [\phi_{0k}(f_{nd}), \ \phi_{1k}(f_{nd}), \ \cdots, \phi_{N-1,k}(f_{nd})]^T = [A_{0k}\theta_{0k}a_{t0}, A_{1k}\theta_{1k}a_{t1}, \cdots, A_{N-1,k}\theta_{N-1,k}a_{t,N-1}]^T$$

and so T_{kt} can also be expressed as follows:

$$T_{kt} = T_t \odot M_k \quad (6)$$

here $\odot$ refers to the Hadamard matrix products and

$$M_k = [A_{0k}\theta_{0k}, \ A_{1k}\theta_{1k}, \cdots, \ A_{N-1,k}\theta_{N-1,k}]^T$$

Compared with T_t above, T_{kt} can be regarded as a result of the target frequency response sample vector T_t modulated with a complex-value vector M_k. It should be noteworthy that M_k completely depends on the interaction between target temporal snapshot vector and Doppler filter weight vector, having nothing to do with the target scattering characteristic. As a result, M_k is the only cause of the distortion of a moving target's FSRP. Next, we will analyze separately the effects of the amplitude and phase term in M_k on FSRP.

The amplitude term effect on FSRP: According to Eq. 5, the amplitude term in M_k can be expressed as:

$$A_{nk}(f_{nd}) = A_k(f_{0d} + n\Delta f_d) = \frac{\sin\{\pi[f_{0d} + n\Delta f_d - kf_r/M]MT_r\}}{\sin\{\pi[f_{0d} + n\Delta f_d - kf_r/M]T_r\}} \quad n = 0\sim N-1 \quad (7)$$

where, $A_k(f)$ is the amplitude passband characteristic of the kth Doppler filter. An amplitude vector can be attained by collecting the amplitude term in M_k as follows:

$$A_k = [A_k(f_{0d}), \ A_k(f_{0d} + \Delta f_d), \cdots, A_k(f_{0d} + (N-1)\Delta f_d)]^T \quad (8)$$

In Eq. 8, for a stationary target ($v_t = 0$), $\Delta f_d = 0$ and all terms in A_k are the same constants and thus do not cause the distortion of FSRP. For a non-stationary target ($v_t \neq 0$), however, as shown in Eq. 8, an additional Doppler frequency shift

$$\Delta f_d = \frac{2v_t}{c}\Delta f$$

is produced between adjacent amplitude elements, thus causing the amplitude fluctuation in A_k.The fluctuation range is decided by the frequency position of $f_{nd} = f_{0d} + \Delta f_d$ (n = 0~N-1) as well as the amplitude passband characteristic of Doppler filter. When performing imaging processing (i.e., IDFT), if effects of the phase terms in M_k are ignored, the role of the amplitude fluctuation in A_k is equivalent to weighting the target frequency response sample vector T_t by asymmetrically amplitude weight vector A_k. Some simulation results provided by Berizzi *et al.* (2008) show that such an asymmetrically amplitude weight can cause the Point Spread Function (PSF) spreading and furthermore the losses of signal-to-noise (SNR); however, no effects upon the correct range location of the FSRP. In practical application, such adverse effect on distortion can be negligible if the fluctuation range in A_k is less than 3dB.

To explain more explicitly, here we can define the N Doppler frequencies f_{nd}, n = 0~N-1 as a band-pass comb-like signal which covers the frequency range $[f_{0d}, f_{n-1d}]$ and has the properties that the interval among frequency components is Δf_d and its bandwidth equals to $(N-1)\Delta f_d$. Then, as shown in Fig. 3, A_k is the result of this band-pass comb-like signal passing through the filter with frequency response $A_k(f)$. Such a definition will greatly simplify the following analysis process. Note that this band-pass comb-like signal's frequency location and bandwidth depend on the target radial velocity v_t.

In Fig. 4a, there are three velocities ($v_{t1}<v_{t2}$ v_{t3}) for target, respectively corresponding to three band-pass comb-like signals in Fig. 4b, d and f. As shown in the Fig. 4a-g, the locations of those band-pass comb-like signals in frequency domain are different, whose bandwidths become larger with the increase of the target velocity.

Since, the half-power width of $A_{nk}(f)$ is approximately equal to f_r/M, we can consider that the range of the amplitude fluctuation is less than 3dB and thereby the distortion caused by the amplitude fluctuation is acceptable if the bandwidth of the band-pass comb-like signal satisfies the condition:

$$\left|(N-1)\Delta f_d\right| \le f_r / M \tag{9}$$

It is worth noting that condition in Eq. 9 is a necessary but not sufficient condition for the acceptable

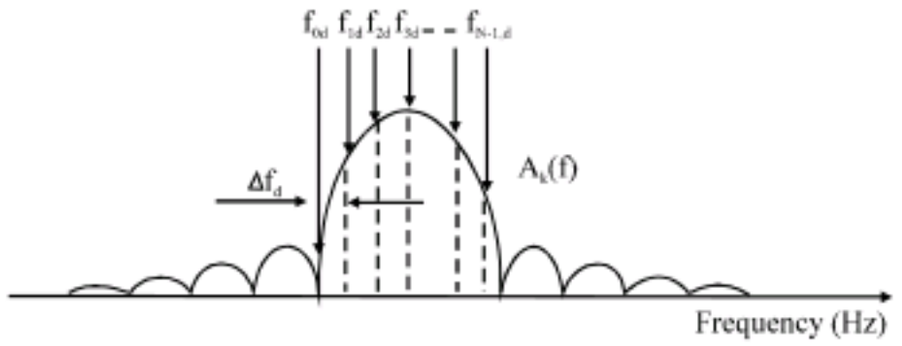

Fig. 3: The relationship between the filter amplitude response characteristic of Doppler filter and N target Doppler frequencies across N subbands

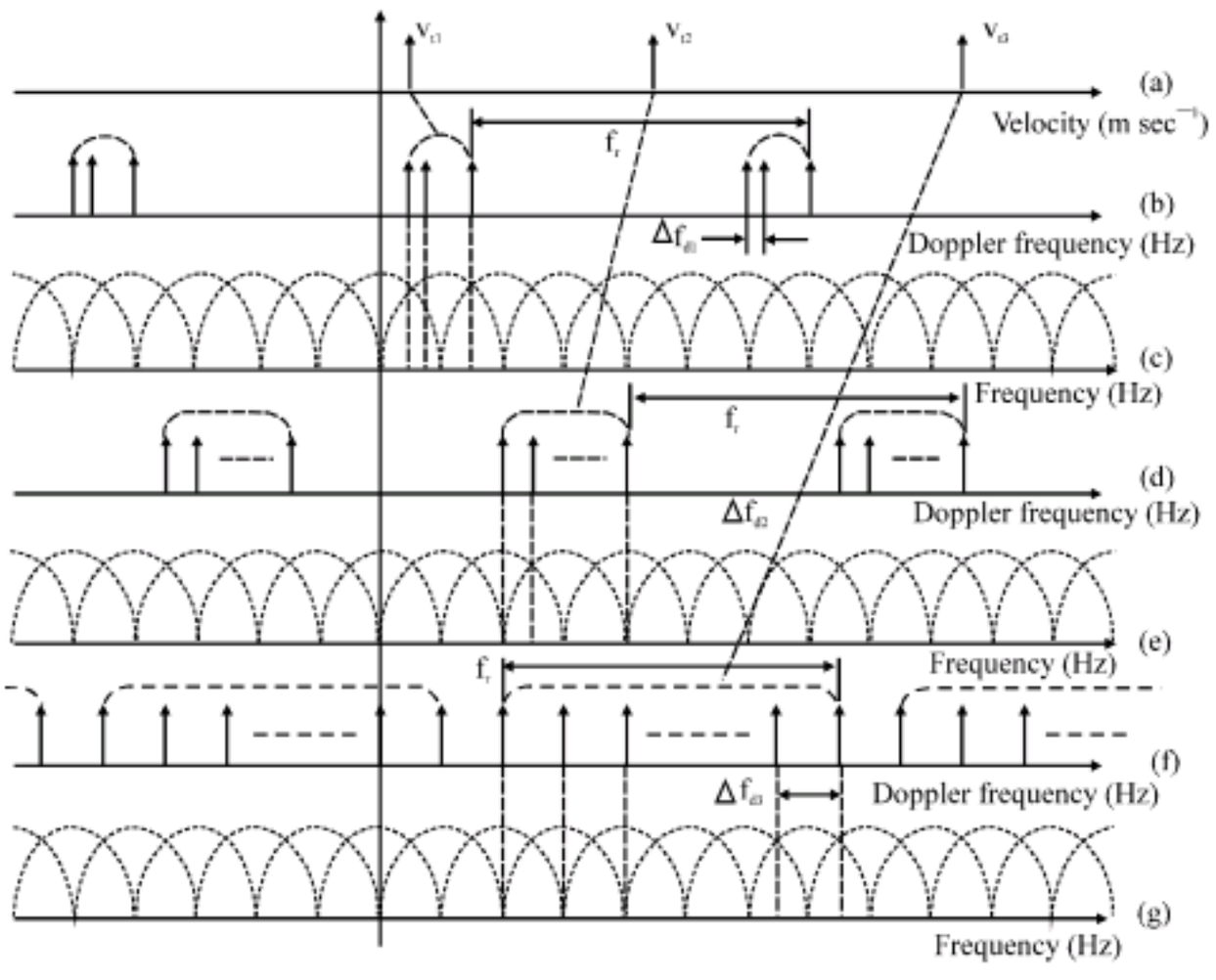

Fig. 4: (a-g) Change in target velocities versus the Doppler filter bank(the sidelobe structures of the filter is not shown)

distortion because the amplitude fluctuation depends not only on the bandwidth of the band-pass comb-like signal but also on the relative position between the band-pass comb-like signal and filter amplitude response. According to the previous analysis, the frequency position of the band-pass comb-like signal varies as the corresponding target's velocity changes.

Figure 5 shows the relative relationship between amplitude fluctuation and two adjacent Doppler filter's amplitude response when the band-pass comb-like signal lies in different frequency positions. From the Fig. 5a-d, we can see that, when the band-pass comb-like signal lies in a Doppler filter's passband with its bandwidth less than the half of the half-power width of the Doppler filter, the amplitude fluctuation range in this Doppler filter can be approximately considered to be less than 3dB. So, a necessary and sufficient condition with even stricter constraint than that in Eq. 9 is then given by:

$$\left|(N-1)\Delta f_d\right| < f_r / 2M \tag{10}$$

Substituting

$$\Delta f_d = \frac{2v_t}{c}\Delta f$$

into Eq. 10, we can obtain the target's maximum critical velocity:

$$\left|v_t\right| < cf_r / 4M(N-1)\Delta f = cf_r / 4M(B-\Delta f) \tag{11}$$

where, $B = N\Delta f$ is the radar system synthetic bandwidth. From Eq. 11, the target' maximum critical velocity can determine the velocity scope of application for the filter bank architecture using FFT.

The phase term effect on FSRP: According to Eq. 5, the phase terms in M_k is:

$$\theta_{nk}(f_{nd}) = \theta_{nk}(f_{0d} + n\Delta f_d) = \pi[f_{0d} - kf_r/M](M-1)T_r + n\Delta f_d(M-1)T_r \qquad n=0\sim N-1 \tag{12}$$

Here, the distortions of FSRP due to the phase term can be better interpreted if Eq. 12 is obtained by sampling the continuous frequency spectrum θ_{nk} of Eq. 13 at $f = n\Delta f_d T_r$, n = 0,1,..,N-1. The analytical expression of $\theta_{nk}(f)$ is hereunder reported:

$$\theta_{nk}(f) = \pi[f_{0d} - kf_r/M](M-1)T_r + \pi[(M-1)f] \tag{13}$$

In Eq. 12, $\theta_{nk}(f_{nd})$ consists of two terms. One is $\pi[f_{0d}-kf_r/M](M-1)T_r$, which is a constant phase term and thus has no effect on the distortions of FSRP. The other is $n\Delta f_d(M-1)T_r$, or a linear phase term, which can cause the range shift of FSRP. According to digital signal processing theory (Oppenheim and Schafer, 2005), the range shift value L can be deduced:

$$L = \lfloor v_t N\Delta f(M-1)T_r / c \rfloor = \lfloor N(M-1)\Delta f_d T_r / 2 \rfloor = \lfloor v_t B(M-1)T_r / c \rfloor \tag{14}$$

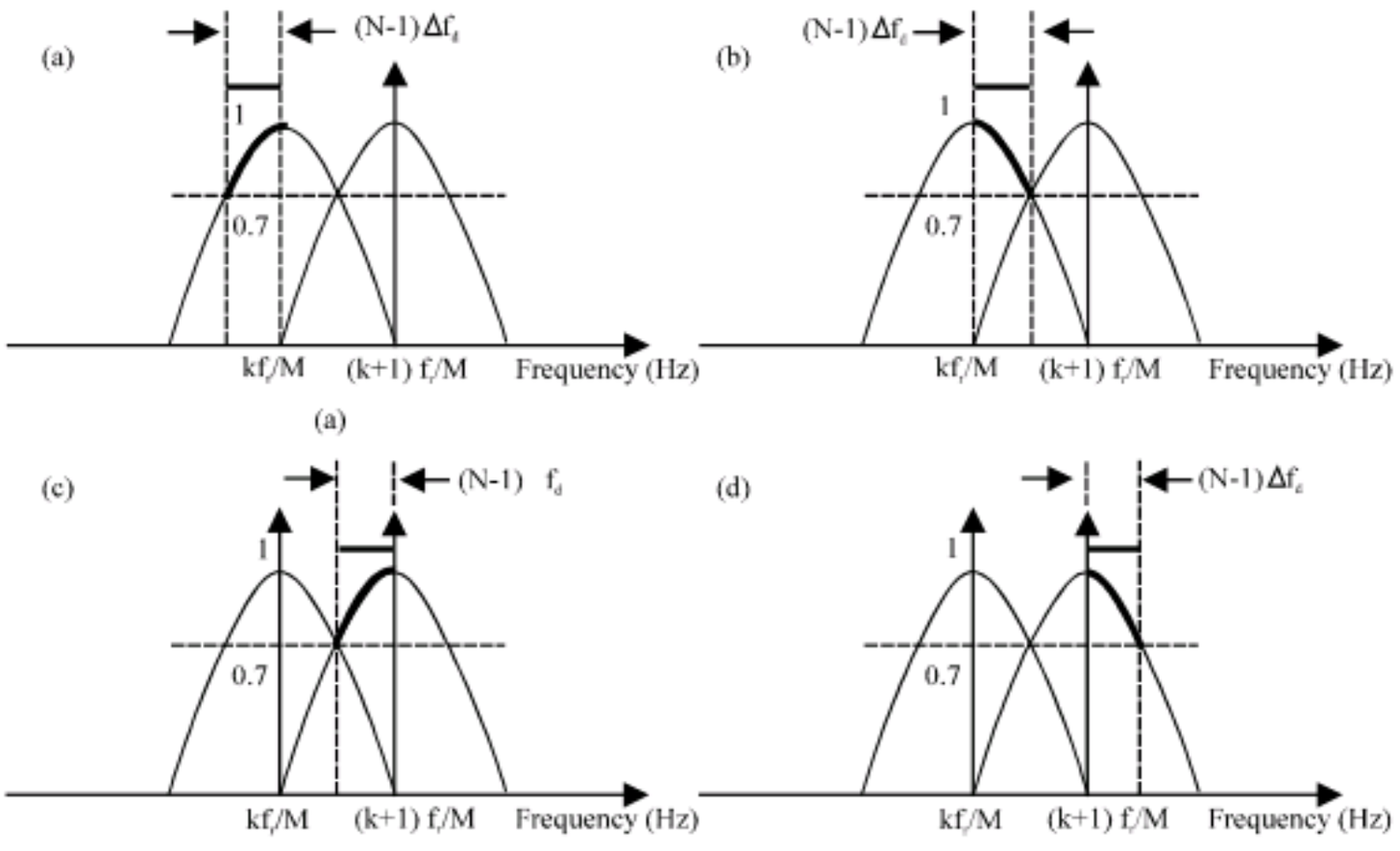

Fig. 5: (a-d) Sketch of the relationship between the band-pass comb-like signal and two adjacent Doppler filter amplitude response (the sidelobe structures of the filter is not shown)

where, [...] denotes the round-off operation. The equation above shows that the range shift produced by linear phase term can map the target's range profile into an incorrect position in the range. Nevertheless, the range profile shape is not altered. When target approaches the radar, then $\Delta f_d>0$ and FSRP shifts L to the left. On the contrary, when target recedes from the radar, then $\Delta f_d>0$, FSRP shifts L to the right.

SIMULATION

In following simulations, we consider one rigid target with uniform radial motion. The radar is assumed to be operating with a start frequency of f_0 = 5 GHz. Subband bandwidth and center frequency interval are denoted by ΔB and Δf, respectively and $\Delta f = \Delta B$ = 10 MHz. When subband number is N = 64, radar system synthetic bandwidth is $B = N\Delta f$ = 640 MHz and corresponding fine range resolution is obtained $\Delta R = c/2N\ \Delta f$ = 0.2344 m. When the PRF is f_r = 5000 Hz and the pulse number in one CPI M = 20, the Doppler bin width can be calculated f_r/M = 250 Hz.

Simulation consists of three parts. The first part is to evaluate the proposed system's wideband target detection performance. The second part is to simulate the relationship between target's velocity and Doppler filter amplitude response in order to demonstrate the validity of the related analysis above. The last is to verify the amplitude term and phase term effects on FSRP distortion.

The relationship between wide detection performance and target velocit: The result of the first part simulation is shown in Fig. 6. In this example, we consider target as a single point scatter with unit amplitude. As shown in the Fig. 6, the synthetic target power is a function of target velocity, whose shape shows a form of fluctuation and peaks gradually decrease with the increase of velocity.

Since, the target power is directly related to detection performance, Fig. 6 reveals the relationship between the target wideband detection performance and target velocity. It is worth noting that according to foregoing analysis, velocity increase only causes the detection performance to decrease, instead of the unacceptable shape distortion of FSRP when the target velocity is less than maximum critical velocity.

The relationship between the target velocity and Doppler filter amplitude response: From Eq. 11, the target's maximum critical velocity is calculated to be 29.76 m sec^{-1}. when target velocity is equal to the maximum critical velocity, 64 Doppler frequency values range from 993 to 1118 Hz and thus the corresponding band-pass comb-like

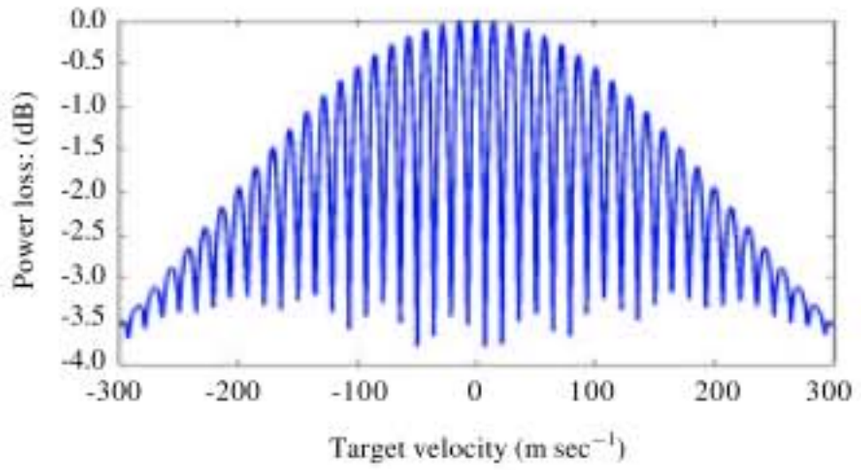

Fig. 6: Single point scatter power loss versus target velocity

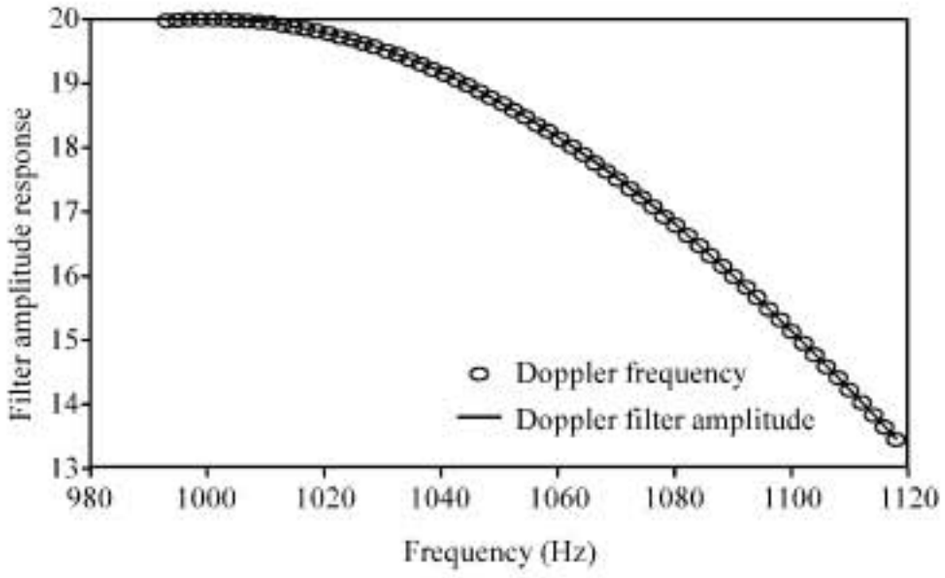

Fig. 7: The band-pass comb-like signal versus filter amplitude response (target velocity 29.76 m sec^{-1}

signal covers frequency range from 993 to 1118 Hz with its bandwidth 125 Hz. Therefore the comb-like signal bandwidth equals to a half of the Doppler bin width. As shown in Fig. 7, the corresponding Doppler filter amplitude response covers range from 13.44 to 20 and its amplitude fluctuation range is approximately equal to 3 dB.

In Fig. 8, when target velocity is twice the maximum critical velocity (59.52 m sec^{-1}), the corresponding band-pass comb-like signal covers frequency range from 1986 to 2236 Hz whose bandwidth of 250 Hz just equals to the Doppler bin width. As shown in the Fig. 8, the corresponding filter amplitude response covers range from 1.5 to 20. The amplitude fluctuation range exceeds 3 dB.

In Fig. 9, when target velocity is 123.35 m sec^{-1}, the corresponding band-pass comb-like signal covers frequency range from -884.3 to -366.2 Hz and its bandwidth 518.2 Hz, is larger than the Doppler bin width. As shown in the Fig. 9, the corresponding filter amplitude response covers range from 0 to 20 and thus the amplitude fluctuation range is larger than 3 dB.

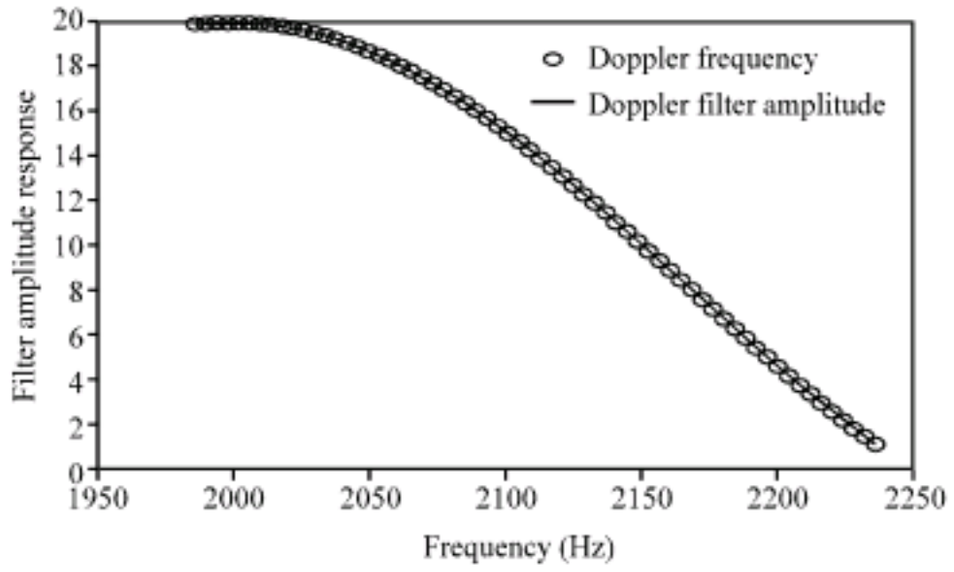

Fig. 8: The band-pass comb-like signal versus filter amplitude response (target velocity 59.52 m sec^{-1})

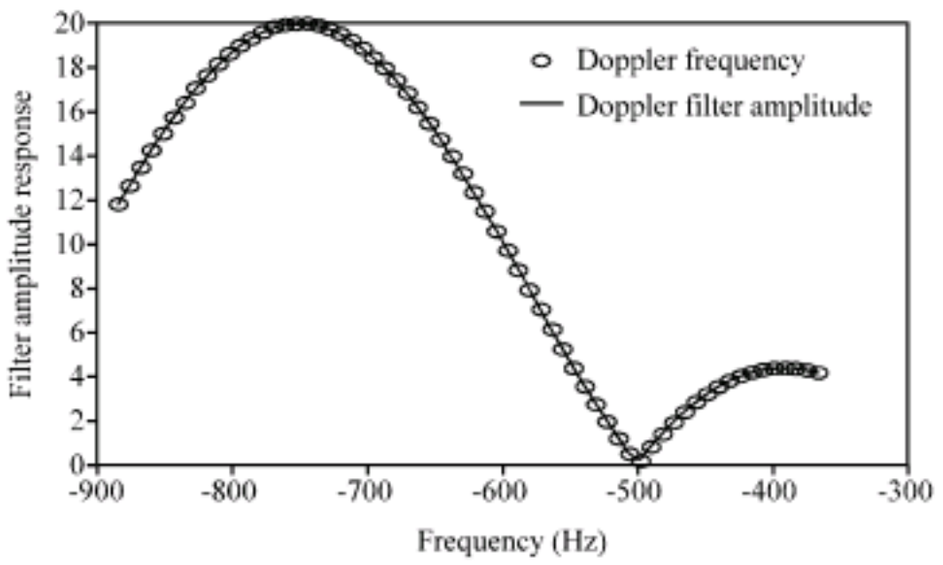

Fig. 9: The band-pass comb-like signal versus filter amplitude response (target velocity 123.35 m sec^{-1})

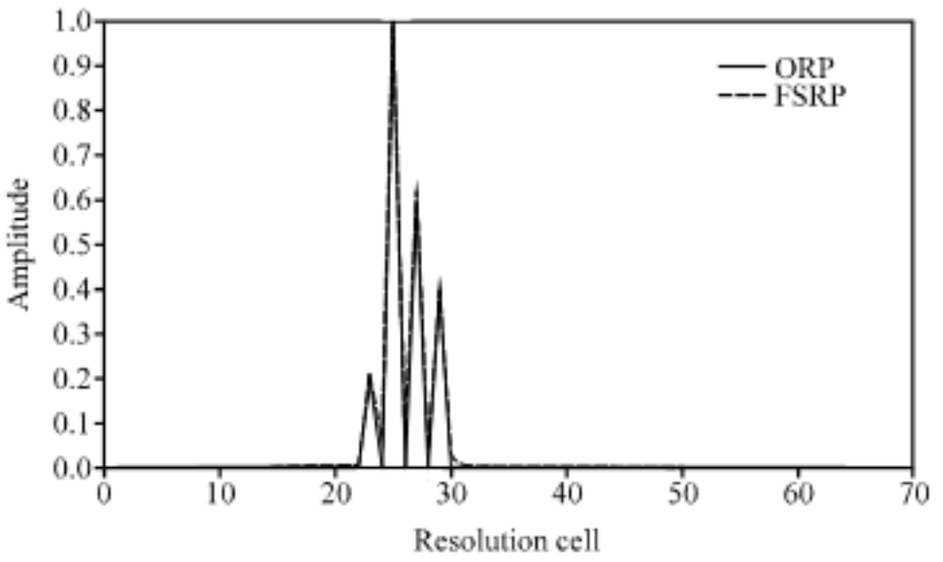

Fig. 10: The amplitude term effect on the FSRP (target velocity 29.76 m sec^{-1})

The amplitude term effect on FSRP: In the simulation below, assume this target includes four scattering centers, i.e., A, B, C and D who are spaced 2ΔR in range from each other. Their relative normalized scattering intensity is 1:5:3:2. The first scattering center of this target is 450 km+22ΔR away from the radar.

The calculated target's maximum critical velocity is 29.76 m sec^{-1}. Figure 10 shows an example of the shape

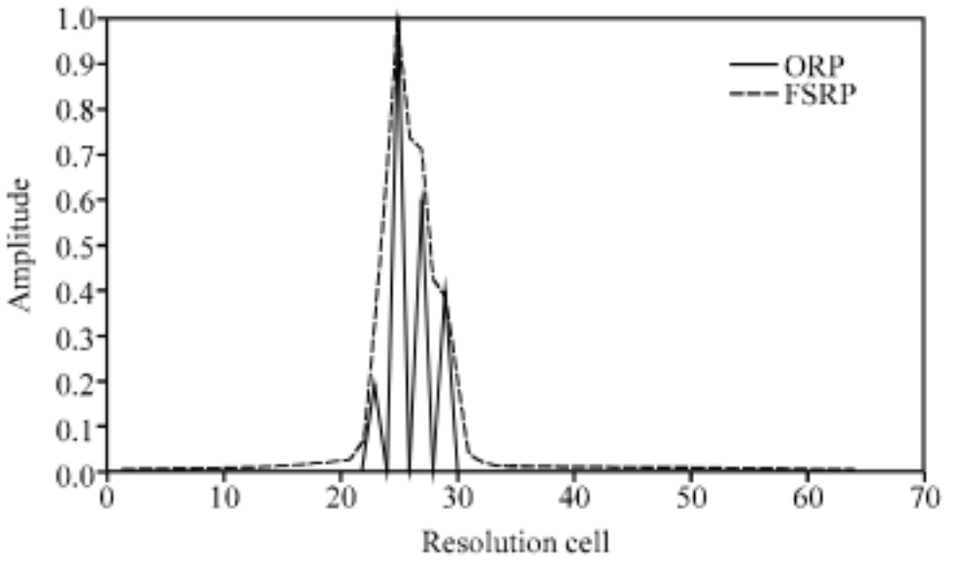

Fig. 11: The amplitude term effect on the FSRP (target velocity 123.35 m sec^{-1})

distortion of FSRP provoked by the amplitude fluctuation when target's velocity is at maximum critical velocity. It is worth pointing out that in Fig. 10 and 11, the phase term effect are ignored in order to better illustrate the amplitude fluctuation effect.

In Fig. 11, the target velocity is 123.35 m sec^{-1}. As compared with the ORP in the Fig. 11, there are significant broadenings of peaks of the FSRP (dashed-line). As analyzed previously, such broadenings occur because the amplitude fluctuation range exceeds 3 dB. By comparison with Fig. 10, the target with the maximum critical velocity produces a higher fidelity profile, having a distinct peak and corresponding well with ORP features (scatter centers location, number, relative amplitude, etc). It is worth noting that in Fig. 11, the range position of FSRP keeps stationary in spite of a significant deformation in its shape.

The phase term effect on FSRP: Figure 12 and 13 show the distortion effect provoked only by the phase term when target's velocities are at 29.76 m sec^{-1} (maximum critical velocity) and 123.35 m sec^{-1}, respectively. In these Fig. 12 and 13, the amplitude fluctuation effect is ignored so as to better understand the phase term effect on FSRP.

According to previous analysis, the phase term causes only the range shift of FSPR rather than its shape of deformation. In Fig. 12, the distortion appears due to the range shift value is not an integer and the corresponding distortionless FSPR can be obtained with interpolation processing. From Eq. 14, the velocity making ORP left shift for a resolution cell is calculated to be 123.35 m sec^{-1}. The corresponding simulation result is shown in Fig. 13. As shown in the Fig. 13, there is no shape distortion in the FSRP (dashed-line) except that the range position of FSRP produces left shift for a resolution cell. All these convincingly prove our previous analysis.

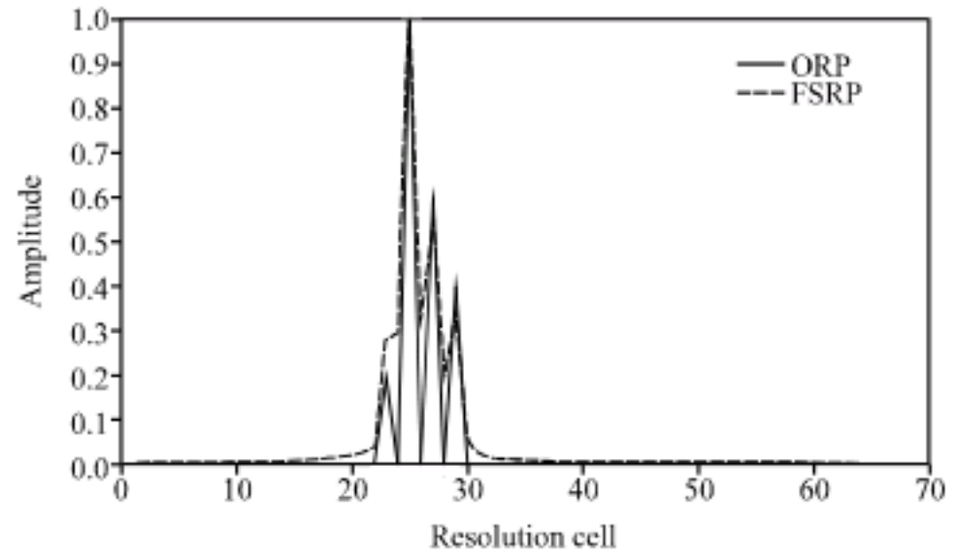

Fig. 12: The phase term effect on the FSRP (target velocity 29.76 m sec^{-1})

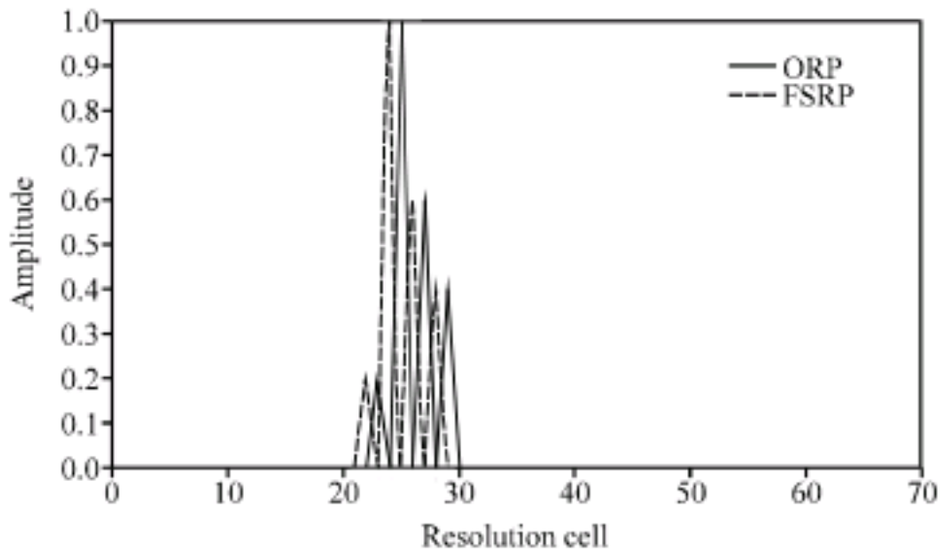

Fig. 13: The phase term effect on the FSRP (target velocity123.35 m sec^{-1})

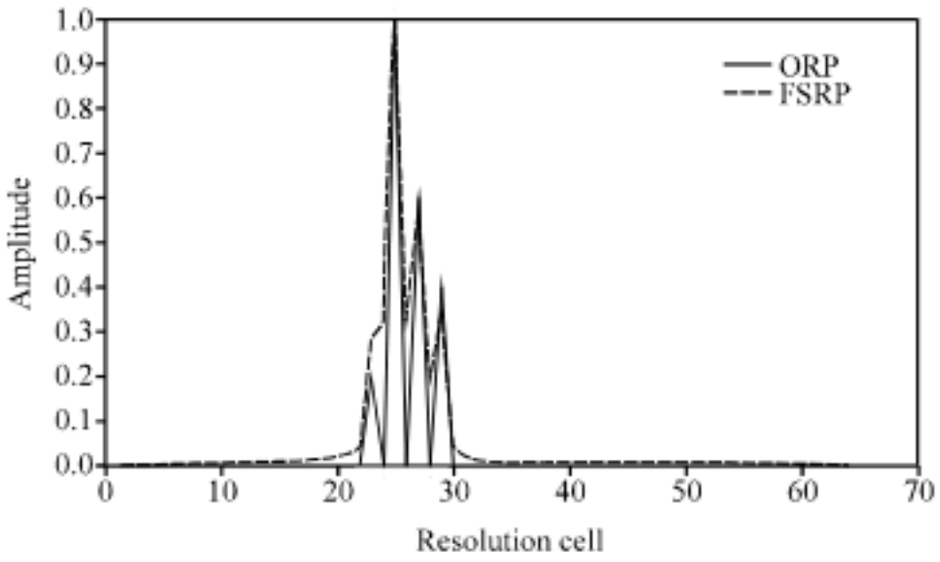

Fig. 14: The joint effect of the amplitude and phase term on the FSRP (target velocity 29.76 m sec^{-1})

The joint effect of amplitude and phase term on the FSRP: The joint effect of the amplitude and phase terms on the FSRP is shown in Fig. 14 and 15 when target velocities are 29.76 and 123.35 m sec^{-1}, respectively.

As compared with the plots in Fig.10 and 12, the distortion of FSRP (dashed-line) in Fig. 14 is almost the same as that of FSRP in Fig. 12. This simply indicates that the distortion under such condition is mainly caused by phase term with negligible amplitude fluctuation effect. On the other hand, the shape of FSRP in Fig. 15 is the same as that of FSRP in Fig. 11 except with a left shift for a resolution cell, which testifies the fact that under such condition the amplitude fluctuation is related exclusively to the shape distortion of FSRP, whose range position comes under effect from phase term.

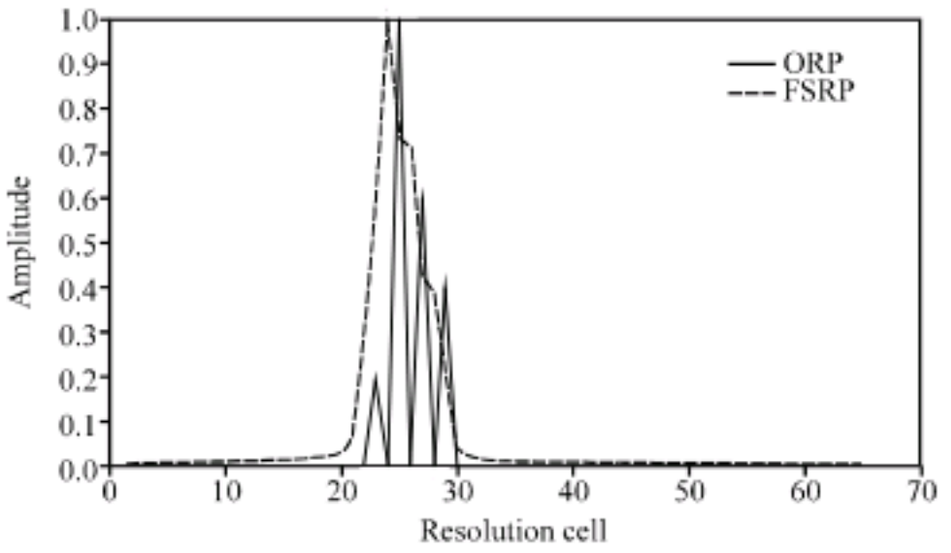

Fig. 15: The joint effect of amplitude and phase term on the FSRP (target velocity 123.35 m sec^{-1})

CONCLUSION

In this study, we propose and analyze a wideband imaging radar system based on conventional Doppler filter bank architecture. The main results of theoretical analysis and simulation are as follows:

- The detection performance of proposed system is the function of target velocity whose detection performance degrades with the target velocity increase
- Doppler dispersion produces the distortion of FSRP. Specifically, the effect on the distortion of FSRP includes two factors: the amplitude term and phase term
- The amplitude term fluctuation only produces the FSRP's shape deformation but keeps the range profile position fixed. The phase term causes profile range shift but has no effect on the shape deformation. The distortion extent caused by both amplitude and phase terms depends on target velocity, radar system synthetic bandwidth, PRF and the pulse number in a CPI
- Two mathematical expressions are deduced not only for the calculation of the range shift value, but also for the evaluation of the amplitude deformation extent when target is in uniform radial motion. Moreover, the maximum critical velocity is derived to determine the velocity scope of application for this proposed imaging architecture

ACKNOWLEDGMENT

This research is sponsored by the National Natural Science Foundation of China under Grant No. 60702070.

REFERENCES

Chen, H.Y., Y.X. Liu, X. Li and G.R. Guo, 2007. Mathematics of synthesizing range profile. IEEE Trans. Signal Process., 55: 1950-1955.

George, W.S., 1998. Introduction to Airborne Radar. 2nd Edn., SciTech Publishing, Inc., Mendham, New Jersey, USA.

Hoffman, A. and S.M. Kogon, 2000. Subband STAP in wideband radar system. Proceedings of the IEEE International Conference on Sensor Array and Multichannel Signal Processing Workshop, Mar. 16-17, Cambridge, MA, USA., pp: 256-260.

Jouny, I. and E. Culpepper, 1994. Adaptive hot clutter mitigation using subbanding. Proceedings of the IEEE-SP International Symposium on Time-Frequency and Time-Scale Analysis, Oct. 25-28, Philadelphia, PA, USA., pp: 476-479.

Linde, G., 2000. Use of wideband waveforms for target recognition with surveillance radars. Proceedings of the IEEE International Radar Conference, May 7-12, Alexandria, VA, USA., pp: 128-133.

Malas, J.A., K.M. Pasala and J.J. Westerkamp, 2002. Wideband radar signal modeling of ground moving targets in clutter. Proceedings of SPIE-The International Society for Optical Engineering, Apr. 1-3, Orlando, FL, USA., pp: 324-335.

Malas, J. A., K.M. Pasala and J.J. Westerkamp, 2004. Automatic target classification of slow moving ground targets in clutter. IEEE Trans. Aerosp. Electron. Syst., 40: 190-205.

Morgan, D.R. and J.C. Thi, 1995. Delayless subband adaptive filter architecture. IEEE Trans. Signal Process., 43: 1819-1830.

Oppenheim, A.V. and R.W. Schafer, 2005. Discrete-Time Signal processing. 2nd Edn., Prentice-Hall Inc., Englewood Cliffs,.

Peng, W., X.G. Wang and J.H. Zhao, 2008. Methods of eliminating doppler dispersion in synthetic wideband signal. Proceedings of the International Conference on Microwave and millimeter Wave Technology, Nanjing, China, Apr. 21-24, IEEE Computer Society, pp: 1540-1543.

Perry, R.P., R.C. Dipietro and R.L. Fante, 1999. SAR imaging of moving targets. IEEE Trans. Aerosp. Electron. Syst., 35: 188-200.

Pillai, S.U., K.Y. Li and J.R. Guerci, 2007. Effect of bandwidth on wideband-stap performance. Proceedings of the 41st Asilomar Conference on Signals, Systems and Computers, Pacific Grove, CA, USA., Nov. 4-7, IEEE Computer Society, pp: 2195-2198.

Rabideau, D.J., 2002. Nonlinear synthetic wideband waveforms. Proceedings of the IEEE Radar Conference, Apr. 22-25, Institute of Electrical and Electronics Engineers Inc., California, USA., pp: 212-219.

Sekiguchi, T. and Y. Kharasawa, 1998. CMA adaptive array antennas using analysis and synthesis filter banks. IEICE Trans. Fundam. Electron. Commun. Comput. Sci., 8: 1570-1577.

Torres, J.A., R.M. Davis, J.D.R. Kramer and R.L. Fante, 2000. Efficient wideband jammer nulling when using stretch processing. IEEE Trans. Aerosp. Electron. Syst., 36: 1167-1178.

Walbridge, M.R. and J. Chadwick, 1999. Reduction of range ambiguities by using irregularly spaced frequencies in a synthetic wideband waveform. Proceedings of the IEE Colloquium on High Resolution Radar and Sonar, May 11-13, Institution of Engineering and Technology, London, UK., pp: 9-14.

Wehner, D.R., 1995. High-Resolution Radar. 3nd Edn., Artech House Inc., Norwood MA., ISBN: 0-89006-727-9.

Whelan, D.A., A. Filip, J.J. Koss, T. Kurien and G. Pappas, 2000. Global space-based ground surveillance: Mission utility and performance of discoverer II. Proceedings of the IEEE Aerospace Conference, Big Sky, MT, USA., Mar. 18-25, Institute of Electrical and Electronics Engineers Computer Society, pp: 1-11.

Yuan, C.H., S.D. Azimi, R. Mahmood, J. Wilbur and G.J. Dobeck, 2000. Underwater target detection using multichannel subband adaptive filtering and high-order correlation schemes. IEEE J. Oceanic Eng., 25: 192-205.

Zatman, M., 1998. How narrow is narrowband?. Proceedings of the IEE Radar, Sonar and Navigation, 1998, IEE, Stevenage, UK., pp: 85-91.